# Role of rift maturity on the architecture and shortening distribution in mountain belts

Anthony Jourdon, Laetitia Le Pourhiet, Frédéric Mouthereau, Emanuel Masini

# Role of rift maturity on the architecture and shortening distribution in mountain belts

Anthony Jourdon[1], Laetitia Le Pourhiet[2], Frederic Mouthereau[1], Emanuel Masini[3]

1- CNRS, GET, Unversité Paul Sabatier, Toulouse, France

2- Sorbonne Université, CNRS-INSU, Institut des Sciences de la Terre de Paris, ISTeP UMR7193, Paris, France

3- Total SA, R&D, Pau, France

## Abstract

Many relic of passive margin are found in mountain belts sometimes together with pristine exhume mantle. The reasons why these structures are preserved from tectonic reworking and whether the piece of mantle that accompanies them is exhumed during extension or collision remains a question. Using thermo-mechanical modelling we find on the one hand that, the strain distribution in the orogenic wedge is controlled by the original position of crustal domains across the rifted margin. In the upper plate, the structural relationships acquired during the rifting phase between the upper mantle and surrounding units are never reactivated during compression due to crustal strain localization. Mantle exhumation on the other hand can occur either during the collision or rifting phase depending on the thermal regime at the onset of the inversion. Applying these general rules to the Pyrenees, we show that exhumed mantle domain in the former passive margin could not exceed a width of 50 km to 70 km; otherwise obduction would have occurred due to the high thermal regime at the onset of the inversion.

## 1. Introduction

The impact of inherited mechanical properties of the lithosphere is recognized to be a major driver in the evolution of orogenic belts (Beaumont et al., 2009; Calignano et al., 2015a; Chenin et al., 2017; Heron et al., 2016; Jourdon et al., 2017; Manatschal et al., 2015; Velasque et al., 1989; Yamato et al., 2008). Geological, geophysical and numerical modelling studies show for instance that age-dependent properties of the lithospheric mantle and crust control first-order patterns of shortening distribution, cyclical evolution and seismicity in orogens (Audet and Bürgmann, 2011; Mouthereau et al., 2013). While lateral heterogeneities in the lithospheric mantle control the location of intracontinental orogenic belt (Calignano et al., 2015b; Heron et al., 2016), the local mechanical coupling between crust and mantle or within the crust controls the tectonic style (Jourdon et al., 2017; Lafosse et al., 2018).

In the recent years, an increasing number of studies have found evidence that structure and timing of tectonic evolution of Alpine-type orogens largely inherit the properties and architecture of former rifted margins. For instance, the onset of fast exhumation and abrupt changes in the thermal structure of orogens point to the accretion of stronger, less thinned segment of rifted margins, as shown in the Zagros (Ballato et al., 2010; Mouthereau et al., 2012), Taiwan (Mesalles et al., 2014) or the Pyrenees (Mouthereau et al., 2014; Vacherat et al., 2016, 2014). An important step forward in the exploration of these relationships have been reached thanks to new high-resolution seismological imaging techniques showing the nature of the mountain root and lateral segmentation of an orogenic system can preserve first-order tectonic features of a rift system (Wang et al., 2016), which confirm former inferences from field geology in the Pyrenees (e.g. Jammes et al., 2009; Lagabrielle and Bodinier, 2008).

However, we still have a poor understanding of the key physical processes at play during the earliest stages of collision, when the distal part of a rifted margin is accreted to form mountain

ranges. Only a limited number of orogens preserve markers of this transient stage in a continuum of laterally evolving geodynamic settings from subduction to collision. For instance, the complex structure of high-pressure units in the Alps (Beltrando et al., 2014) and the formation of non-metamorphic ophiolitic mélange in the Alps or the Pyrenees (Beltrando et al., 2014; Lagabrielle and Bodinier, 2008; Müntener et al., 2009) display end-members expression of inverted hyper-extended domain of magma-poor margins. Here, we focus on the role played by the size, number and vergence of detachment zones, thermal maturity and the overall architecture of a rifted margin on the accretion of the hyper-extended domain preserved in collisional belts. Using numerical models we try to get a better understanding on how, where and when rift inherited structures are reactivated throughout the collisional orogenic process and whether exhumed mantle units preserved in mountain belts related to rifting, orogeny or both. The study focuses primarily on the effect of the maturity of the margin, i.e. the residual rift thermal anomaly, on the structure of the nascent mountain belt.

## 2. Natural constraints for inverted rifts from the Pyrenees

The Pyrenean belt is probably one of the best documented examples of an inverted rift system. The shortening of the former extensional domains with different rift maturities/width along strike resulted in the preservation of different stages of orogeny along strike. The Bay of Biscay fossilized a nascent subduction zone involving an oceanic domain with a classical oceanic crust. Eastward, the convergence in the Pyrenees led to a fully developed orogenic wedge (Figure 1b). The role of rift segmentation is reflected across the Pyrenees as in the Mauléon basin where a former rift structure is interpreted as an inverted hyper-extended margin with an exhumed mantle domain (Jammes et al., 2009; Lagabrielle et al., 2010; Lagabrielle and Bodinier, 2008; Masini et al., 2014; Teixell et al., 2016; Tugend et al., 2014; Wang et al., 2016), while the eastern part of the belt shows a more complex pattern of

discontinuous exhumed mantle zones (Figure 1b; Grool et al., 2018; Vacherat et al., 2014). According to paleogeographic reconstructions (Jammes et al., 2009; Tugend et al., 2014; Nirrengarten et al., 2018), a major transtensional rifting phase started in the Late Jurassic-Early Cretaceous (~150-120 Ma). Extension between Europe and Iberia was first distributed between the Central Iberian Belt and the Pyrenees. Then, rifting localized in the Pyrenean domain in the Late Aptian-Albian (~115 Ma) and resulted in mantle exhumation in the North Pyrenean zone (Jammes et al., 2009; Lagabrielle et al., 2010; Lagabrielle and Bodinier, 2008; Masini et al., 2014; Teixell et al., 2016; Tugend et al., 2014). The late stages of rifting are marked by a HT-LP metamorphism (Albarède and Michard-Vitrac, 1978; Montigny et al., 1986). It corresponds to a strong thermal anomaly affecting both pre- and syn-rift sediments that locally exceed 600°C in sedimentary basins close to exhumed mantle domains (Clerc et al., 2012; Ducoux, 2017; Vacherat et al., 2014). Vacherat et al. (2014) showed that the rift-inherited thermal anomaly prevailed as convergence started in Late Cretaceous, which supports a fast plate boundary inversion with no evidence for thermal relaxation.

Pyrenean orogeny is often considered as two-folds (Dumont et al., 2015; Mouthereau et al., 2014). A first early orogenic phase consists of the inversion of former north pyrenean rifts (Dumont et al., 2015; Mouthereau et al., 2014; Tugend et al., 2014; Vacherat et al., 2016) as early as the Santonian (~85 Ma). Incipient orogenic reliefs are also recorded during this phase as evidenced by thermochronology (Vacherat et al., 2016). The second orogenic phase consists in the Eocene-Oligocene crustal nappe-stacking of the Axial zone (Pyrenean high range) corresponding to the main stage of crustal thickening, relief and topographic growth until the early Miocene post-orogenic time (Mouthereau et al., 2014). Although the timing and history of the Pyrenean rifting and orogeny seems to be well constrained, the way the former influence the latter is often postulated but poorly evaluated physically. As a result, first order questions such as wether the actual pre-orogenic width of the exhumed mantle/oceanic

domain between Iberia and Europe in the Pyrenees was 10 km or 200 km remain open, leaving large uncertainty in regional plate kinematic scenario.

## 3. Dynamic modelling of tectonically-inverted hyper-extended rifts

Numerous numerical modelling studies have been performed to understand the role of the rheology and of the properties and architecture of continental lithosphere during collision (Beaumont et al., 2009, 2001; Burg and Gerya, 2005; Burov et al., 2014, 2011, 2001; Duretz et al., 2012; Duretz and Gerya, 2013; Dymkova et al., 2015; Jourdon et al., 2017; Warren et al., 2008; Yamato et al., 2008). However, the majority of these models did not account for the complexity of rifted margins. Based on the Pyrenean study case, studies (Erdös et al., 2014; Jammes et al., 2014; Jammes and Huismans, 2012) showed that the extension phase preceding the collision can explain the observed presence of mantle bodies at shallow depth and that inherited structures facilitate the propagation of the deformation in the orogenic wedge. These models assume narrow rifts with limited amount of extension (thinning factors of about 2). The lack of a large domain with exhumed mantle is at odd with commonly accepted reconstructions of the Pyrenean rifts where extension led to a mature and wide hyper-extended domain but failed to record seafloor spreading. Offshore mapping of rift domains in the Bay of Biscay indeed argued for the occurrence of a 100 km large widespread area of hyper-thinned continental crust, exhumed domains and even oceanic crust (e.g. Tugend et al., 2014). This result accords with geophysical imaging of magma-poor rifted margins showing a 70 to 200 km wide domain of hyper-extended crust, typically thinned below 10 km, sandwiched between the necking zone and a domain of exhumed mantle (e.g. Chenin et al., 2017).

Numerical models which are able to produce such magma-poor hyper-extended margins require a weak crustal channel to decouple crust and mantle which in turn produces a delay in

the necking of the mantle. In 2D, they require slow extension rates (< 1cm/yr) (Brune et al., 2017, 2014; Manatschal et al., 2015; Naliboff et al., 2017; Tetreault and Buiter, 2017) or a mechanically layered lithosphere (Duretz et al., 2016) in which pre-existing softened zones permit to keep the deformation sufficiently distributed during lithospheric thinning to delay the break-up. During the final mantle exhumation phase, the 1200°C (LAB) isotherm typically lies at ~20 km or more beneath a magma-poor type Mid Oceanic ridge axis involving a "cold" rift geotherm (Dick, 1989; Lagabrielle and Lemoine, 1997; Sauter et al., 2013, 2004).

Among these 2D models, the crustal thinning is firstly accommodated by simultaneous faulting, and then followed by a sequential faulting (Brune et al., 2017, 2014; Manatschal et al., 2015; Naliboff et al., 2017; Tetreault and Buiter, 2017) rooting along a main detachment shear zone called "exhumation channel" (Brune et al., 2014) or "viscous channel" (Lavier and Manatschal, 2006) which allows rift migration and the formation of asymmetric rift systems. This process of strain localization along shallow dipping shear zones and rift asymmetry is interpreted as resulting from mechanical softening with ongoing deformation (Huismans et al., 2005; Lavier and Manatschal, 2006).

### *3.1. Rheology*

Our models setup took benefit of former numerical models that were successful in reproducing the formation of magma-poor hyper-extended margins. The initial layering is designed to represent a simplified pre-rift lithosphere. The continental crust is divided in three layers (Figure 2a): (1) the upper crust from the surface to 10 km, (2) the middle crust from 10 km to 20 km and (3) the lower crust from 20 km to 35 km. Upper and middle crust rheology is approximated with a quartz flow law (Table 1, Ranalli and Murphy, 1987) according to the granitic composition of the upper crust (Denèle et al., 2012; Wickham, 1987) while the lower crust rheology is simulated with an anorthite flow law (Table 1, Rybacki and Dresen, 2000)

143 representing a more felsic composition (Wickham, 1987). This layering allows a decoupling
144 between the middle and lower crust (Figure 2b).

145 For all runs, the mantle is divided into two phases: (1) the lithospheric mantle from 35 km to
146 120 km and (2) the asthenosphere from 120 km to 200 km. The rheology of these two phases
147 is modelled with a dry olivine dislocation creep law (Table 1, Hirth and Kohlstedt, 2003).

148 In addition, the brittle parts of the lithosphere are simulated using the Drucker-Prager yield
149 criterion adapted to continuum mechanics (see Supplementary Material). We implement at the
150 beginning of the simulation a random Gaussian distribution (see supplementary material for
151 details) of a small plastic strain amount (0 to 0.4) to simulate an already damaged lithosphere.
152 This initial plastic strain will decrease the friction angle following a linear plastic strain
153 softening (Figure 2c). The plastic strain softening is used to roughly approximate the
154 behaviour of large faults that record long-term slip and localization due to phyllosilicates
155 crystallisation in crustal rocks or serpentinization in mantle rocks.

156 ### *3.2. Thermal setup*

157 The initial thermal state is computed with the analytical solution provided in Burov &
158 Diament (1995), with a radiogenic heat production in the crust of 8.91 $\mu W.m^{-3}$. A thermal
159 perturbation is added at the centre of the domain (Figure 2a). The 1300°C isotherm
160 representing the lithosphere-asthenosphere boundary is located at 120 km and the Moho
161 temperature is 603°C (Müntener et al., 2000) (Figure 2b). The thermal boundary conditions to
162 solve energy conservation are: 0°C at the surface, 1340°C at the bottom of the domain (200
163 km) and null heat flux on the left and right sides of the model.

164 ### *3.3. Velocity boundary conditions*

165 In order to investigate the influence of extensional structures during the collision we simulate
166 an extension phase followed by compression. During the first 30 Myr we impose a constant

extension velocity (Figure 2d and Supplementary material Table S1, given velocity values are the absolute velocity difference between the two model sides). We adopt a 5 Myr window between extension and compression to simulate a smooth plate boundary inversion (Figure 2d) rather than a sharp extension to compression inversion. In detail, model velocity decreases linearly from 30 Ma to reach zero at 32.5 Ma. Then, from 33 to 35 Ma the compression velocity linearly increases to reach 2.5 $mm.yr^{-1}$ and remains constant until the end of the simulation. The extension velocity varies from a model to another in order to investigate the role of along-strike variations of margin width and maturity during mountain building for an extensive system which undergoes the same period of extension.

Our models are not aimed to represent orogenies which went through a long convergence history like the India-Asia hyper-collision in which colliding lithospheres have very different thermo-mechanical properties (Molnar and Tapponnier, 1981, 1975). However, these models represent alpine-type collisional belts, where the upper plate is weakly deformed and structures of the former passive margin are well preserved.

Models presented in this study are performed with pTatin (May et al., 2015, 2014) a parallel implementation of the finite element method, which employs an Arbitrary Lagrangian Eulerian discretization, together with the material point method for the rheologies described in supplementary material. It is coupled to a diffusive surface processes model (see details in Jourdon et al. 2018).

# 4. Results

## *4.1. Structure of hyper-extended domains with variable amount and rates of extension*

All our experiments show the systematic development of lithospheric-scale detachment during rifted margin formation, which number, direction of slip and lateral extent are shown to depend on the amount and rates of extension.

In runs 1 to 3 deformation first localizes at the middle-lower crust boundary. As extension increases the shear zones exhumed through the crust and progressively reach the surface. The decoupling between middle and lower crust is accommodated by a shallow dipping shear zone in both proximal and necking domain during the whole rifting phase. A second decoupling level develops between the lower crust and the mantle. The oceanward sense of shear eventually leads to lower crust extraction in the distal domain resulting in mantle exhumation to upper crustal levels. Depending on the extension velocity, which is equivalent to the total amount of stretching in our model, the final rift structure differs and the geothermal gradient becomes greater with increasing extension velocity. At the end of extension, Run 1 displays an aborted rift system characterized by four antithetic normal fault zones (Figure 3). The most external fault zones are synchronous conjugate shear zones which developed during the first 15 Myrs and constitute the necking domain. Then two sequential shear zones are formed in the centre of the rift. At the end of the rifting phase the mantle is not exhumed and a 10-20 km thick crust remains.

Runs 2 and 3 display more mature passive margin structures and the mantle is exhumed to the surface. During crustal thinning the major part of the deformation is accommodated by crustal normal shear zones in the distal domain connected to a single low-angle detachment dipping oceanward at the Moho and rooting into the mantle in steeply dipping shear zone. This

lithospheric scale detachment represents the upper-lower plate boundary. It is remarkable that once the crust is thinned enough (~5 km thick) the upper-lower plate relationship switches and a second steep mantle detachment of opposite vergence initiates (Figure 4). Run 3 (Figure 5) characterized by more extension, shows a succession of sequentially formed detachments exhuming the mantle asymmetrically along mantle core complex structures. During mantle exhumation, the shear zone flattens until it becomes mechanically easier to create a new detachment rather than continuing to exhume along the previous one. At higher extension velocities, these structures vanish due to a warmer thermal regime which can be assimilated to a mid-oceanic ridge.

### *4.2. Rift inversion and mountain building*

The onset of inversion is accommodated by reactivating former weak crustal extensional shear zones driven by first strain localization in the mantle where the rift thermal anomaly was maximal. The first back-thrust develops in the upper plate 10 to 15 Myrs after the polarity change. Following the onset of continental accretion, the crustal strain propagates into the down going plate along the reactivated middle-lower crust décollement. As the lowermost crust is underthrusted, the middle/upper crust is shortened and thickened to form a typical thick-skinned orogenic wedge. Shortening ratios of each former passive margin domains remain close between the different runs. Indeed, the lower plate hyper-extended domain shortens from 40% to 60%. The lower plate necking domain shortens from 35% to 50% while the upper plate records no shortening up to 30%. Internal deformation within the wedge results in tilting of former thrusts and their passive transport toward the rigid upper plate along the retro-wedge thrust. The mantle exhumed in the upper crust during the rifting acts as a buttress during inversion. The back-thrust plays an important role in the deformation process as it localizes almost all the upper plate shortening. Coupled with orogenic wedge thickening and erosion, it allows exhumation of the deepest units.

In the slowest rift case (run 1; Figure 3) the mantle is not exhumed. However, the lithospheric mantle remains incorporated to the belt at the end of collision. This mantle unit is bordered by a reactivated shear zone, which is the first shortening structure in the crust. The former extensional shear zones which linked the two decoupling levels at middle-lower crust boundary and along the Moho are passively transported in the hanging wall of the retro-wedge thrust, and the extensional relationships between the crust and mantle are preserved. Finally, a second back-thrust is activated during the last steps of the collision and reactivates a former extensional shear zone.

In runs 2 and 3, mantle exhumation during rifting is observed. Larger exhumed mantle domain leads to larger mantle units outcropping in the mountain belt. Run 2 (Figure 4) shows a first back-thrust structure located in the mantle, which is abandoned 20 Myr after the onset of tectonic inversion. A new retro-wedge thrust forms closer to the surface. This thrust nucleates in the mantle and then connects upward into a former extensional shear zone in the crust. This structure accommodates all the upper plate shortening, letting the most distant normal shear zones intact. At the end of the simulation the upper plate preserves most of the architecture inherited from the rifting stage. Once again, the mantle and crust units carried by the retro-wedge thrust exhibit rifting structures which are tilted but not deformed during the collision.

Run 3 (Figure 5) displays a wide exhumed mantle domain (~70 km), which formation was accommodated by extension across 5 detachments. The inversion process starts as in the other runs along a shear zone connecting the thinnest part of the rifted margin with the thermal anomaly in the mantle. As the shortening increases, the margin underthrusts the exhumed mantle assisted by the reactivation of crustal normal faults and mantle detachments. At the end of the experiment, the orogenic wedge is shaped by the underthrusted continental passive

margin and a wide suture zone of obducted exhumed mantle while the upper continental plate is poorly deformed.

# 5. Discussion

## *5.1. Rift architecture*

All our experiments show the systematic development of lithospheric-scale detachment during rifted margin formation, which number, direction of slip and lateral extent are shown to depend on the amount and rates of extension. Detachment structures develop sequentially in the mantle, always landward-dipping regarding the position of the plate boundary. A first detachment is created when the continental crust reaches a thickness less than 5 km. Then, detachments develop regularly every 1 Myr or 2 Myrs and result in regularly spaced structures. This deformation and mantle exhumation sequence is a characteristics of slow-spreading ridges as the southwest Indian ridge (Reston and Mcdermott, 2011; Sauter et al., 2013) and has been imaged in magma-poor conjugate margins of the Newfoundland (Hopper and Funck, 2004) and Iberia (Krawczyk et al., 1996; Reston et al., 2007) margins. Moreover, these detachments can sometimes be found in exhumed mantle or ophiolites as in the Tasna nappe in the Swiss Alps (Froitzheim and Rubatto, 1994; Manatschal, 2014; Reston and Mcdermott, 2011). In the model displaying this detachment sequence (run 3, Figure 5), the obducted mantle exhibits inverted detachment faults.

## *5.2. Thermal structure*

The temperature peak of the rifted margin in the Pyrenees is evaluated between 200°C and 600°C in the pre- and syn-rift sediments (Clerc et al., 2012; Ducoux, 2017; Vacherat et al., 2014). However, the most part of metamorphosed pre- and syn-rift sediments reached 300°C to 350°C (Clerc et al., 2012; Vacherat et al., 2014). In our study, syn-rift sediments undergo

200°C to 330°C, i.e., the average peak temperature recorded in syn-rift Pyrenean sediments. This temperature is limited by the fact that in 2D, wide margins form at small rate of extension promoting cold geotherm or in 3D, the presence of an out of plane propagator also permits to distribute extension at larger rate than in 2D enabling warmer regime to occur at similar crustal thickness and margin width (Le Pourhiet et al., 2018). Alternatively, the presence of highly conductive salt layer in the pre-rift sediment could also have affected the temperature recorded in the sediments and none of the model above account for possible hydrothermal heating.

### *5.3. Mantle exhumation*

Mantle bodies exposed in the Pyrenees are interpreted to be remnants of the subcontinental mantle exhumed during the rifting phase (Lagabrielle et al., 2010; Lagabrielle and Bodinier, 2008). We note, however, that in the case of a small amount of extension as in run 2, the mantle may be exhumed while being passively transported along the retro-wedge. Moreover, either in compression or in extension, the exhumed mantle still displays at the end of the collision the structural patterns acquired during the rifting phase. For instance, the extensional shear zones bounding the exhumed mantle unit are not reactivated. Natural examples of exhumed mantle units incorporated into mountain belts display preserved extensional structures such as the Beni Bousera peridotite in the Rif (Frets et al., 2014) or the Ronda peridotite in the Betics (Précigout et al., 2013). The finding of extensional structures associated with exhumed mantle bodies cannot therefore be considered as a definitive explanation of the main process of mantle exhumation.

### *5.4. Inversion process*

In all runs of this study, inversion is localized on the rift thermal anomaly. Indeed, the upward advection of the isotherms leads to strong temperature-dependent weakening of the

lithospheric mantle through diffusion or dislocation creep. Therefore, when the inversion starts, strain localizes on the weakest part of the domain. One important result is that strain localization controlled by the rifting thermal anomaly triggers the underthrusting of one of the rifted margins beneath the exhumed mantle domain. This result implies that the width of the exhumed mantle domain cannot exceed a certain size, beyond which obduction occurs (Figure 6). In the Pyrenees, the time laps between extension and compression is short and occurs within a high temperature gradient (Masini et al., 2014; Vacherat et al., 2014). Our study shows that such boundary conditions can reproduce a case like the Pyrenean orogeny only for a small (< 50 km) exhumed mantle domain developed between the Iberian and European plates (Figure 6), which is consistent with estimates from Mouthereau et al. (2014).

### *5.5. Preserved rift structures in pro- and retro-wedge sides of the orogen*

The growth of an asymmetric collisional orogenic wedge in our experiments leads to the formation of classical pro- and retro-wedge structures. Such pop-up like orogenic structure is generally well-reproduced in models assuming a kinematic singularity (Jamieson and Beaumont, 2013) and more recently in models accounting for thermal perturbations at the base of the lithosphere (Jaquet et al., 2018). Deformation sequence in the lower plate propagates from the thinnest part of the former hyper-extended domain to the proximal margin. The former hyper-extended domain shortens from 40% to 60%. The deformation is mainly localized on former normal faults. Then, it propagates to the necking domain which shortens around 40% before reaching the proximal domain. Such values are in the range of crustal strains estimated from balanced cross-sections in external orogens (Mouthereau et al., 2013). Our experiments may therefore help geologists estimating shortening values in orogens from the knowledge of the shortening rifted segment. In our models that explicitly account for rift inheritance, the retro-wedge side of the orogen is a direct consequence of extension. Indeed, the upper plate that hosts the retro-wedge is characterized by limited shortening.

Former normal faults are well preserved and the crust is poorly or even not thickened. This behaviour is due to: (i) the small amount of underthrusted mantle limiting heat transfer (or melt) in the upper plate and therefore thermal weakening; (ii) the large amount of exhumed mantle at upper crustal levels acts as a buttress where the retro-wedge structures root; (iii) the ability of the lower plate to deform easily during its underthrusting. Moreover, the former rifting phase strongly influences the deep structure of the belt, particularly beneath the suture zone and the upper plate. Indeed, large mantle bodies exhumed beneath hyper thinned margins are preserved beneath the upper plate and above the crustal root. Otherwise, when the crust remains as thick as in the run 1, the deep structure of the belt exhibits less mantle and a sharp vertical transition from mantle to crust in the suture zone.

## 6. Conclusions

Through thermo-mechanical modelling we are able to provide new constraints and interpretations about the Pyrenean rifting and its influence on the following mountain building stage:

- The rapid extension to compression switch of stress regime accompanied by a hot thermal regime implies that the width of the mantle exhumed domain could not exceed 50 km to 70 km, otherwise obduction of large mantle bodies would have occurred.
- Mantle exhumation during extension is driven by continentward dipping detachment faults developing sequentially at the plate boundary.
- Extensional shear zones that originally developed in the lower plate are reactivated as thrusts while extensional structures of the upper plate are mainly preserved due to strain localization in the lower plate and along the retro-wedge thrust.
- The exhumed mantle incorporated in the mountain belt does not display reactivated normal shear zones. The relationships between the crust and exhumed mantle acquired during the rifted phase are conserved.

- The presence of the mantle in the mountain belt is not necessarily due to mantle exhumation during rifting. Mantle can also exhume during shortening stages. However, models displaying mantle exhumation during extension end with a higher proportion of exhumed mantle in the mountain belt.
- All simulations showed that the shortening amounts are very close regarding the former passive margin domains regardless of the size of those former domains. Once the former passive margin domains identified, this result can help to evaluate the shortening amount in mountain belts when no markers are available.

## Acknowledgement

This study is part of the Orogen program, a tripartite research collaboration between CNRS, BRGM and Total SA. This work was granted access to the HPC resources of CALMIP supercomputing centre under the allocation 2018-P18002. We thank Stefan Schmalholz for his constructive review.

376 # Table

| | Units | Quartz | Anorthite | Olivine |
|---|---|---|---|---|
| Reference | | Ranalli and Murphy 1987 | Rybacki and Dresen 2000 | Hirth and Kohlstedt 2003 |
| A | $MPa^{n}.s^{-1}$ | $6.3x10^{-6}$ | 13.4637 | $1.1x10^{5}$ |
| n | | 2.4 | 3 | 3.5 |
| Q | $KJ.mol^{-1}$ | $156x10^{3}$ | $345x10^{3}$ | $530x10^{3}$ |
| V | $m^{3}.mol^{-1}$ | 0 | $3.8x10^{-5}$ | $18x10^{-6}$ |

377 Table 1

378

379 # Figures captions

380

381 Figure 1: a) Structural map of the Pyrenees (modified from Mouthereau et al., 2014). Thick
382 black dashed lines indicate cross-sections c) and d). Coloured dots indicate the former
383 extensional domains (modified from Tugend et al., 2014). b) Structural sketch map of the
384 Pyrenean rift during the Santonian (~85 Ma, modified from Tugend et al., 2014). c)
385 Geological cross-section of the western Pyrenees interpreted from tomographic model
386 (modified after Wang et al., 2016). d) Geological cross-section of the central Pyrenees
387 (modified from Mouthereau et al., 2014).

388 Figure 2: a) Numerical phases geometry, thermal structure of the models and boundary
389 conditions. b) Yield-stress envelopes computed for a strain rate of $10^{-15}$ $s^{-1}$ for the different
390 materials used to simulate the lithosphere. The Yield-stress envelopes represent the high stress

cutoff used in the simulations (400 MPa). This cutoff is set to roughly approximate the strength limitation for high confinement pressures (Watremez et al., 2013). The red line indicates the initial undisturbed geotherm. c) Plastic strain softening, the friction angle decreases from 30° to 3° with the increase of plastic strain. d) Variation during the runs of the absolute velocity difference between the two model sides. Ext: extension, Comp: compression.

Figure 3: Run 1 evolution. Extension phase velocity of 4 mm/a over 30 Myr. Inversion starts at 35 Myr. Colours of the left panel represent the cumulative plastic and viscous strain. Colours of the right panel represent the numerical phases of the run. Sediments are indicated by 1 Myr alternating colour bands. Black lines represent the extensive shear zones, red lines represent the compressive shear zones and dashed black and red lines represent the reactivated shear zones. The frictional shear zones are drawn for a corresponding plastic strain superior or equal to 1. The viscous shear zones are drawn for a corresponding viscous strain superior or equal to ~1.8-2. Abbreviations represent the passive margin domains, N.D.: Necking domain. Colours are the same than in the horizontal shortening legend.

Figure 4: Run 2 evolution. Extension phase velocity of 5 mm/a over 30 Myr. Inversion starts at 35 Myr. Colours of the left panel represent the cumulative plastic and viscous strain. Colours of the right panel represent the numerical phases of the run. Sediments are indicated by 1 Myr alternating colour bands. Black lines represent the extensive shear zones, red lines represent the compressive shear zones and dashed black and red lines represent the reactivated shear zones. The frictional shear zones are drawn for a corresponding plastic strain superior or equal to 1. The viscous shear zones are drawn for a corresponding viscous strain superior or equal to ~1.8-2. Abbreviations represent the passive margin domains, N.D.: Necking domain, H.E.: Hyper-Extended domain. Colours are the same than in the horizontal shortening legend.

Figure 5: Run 3 evolution. Extension phase velocity of 6 mm/a over 30 Myr. Inversion starts at 35 Myr. Colours of the left panel represent the cumulative plastic and viscous strain. Colours of the right panel represent the numerical phases of the run. Sediments are indicated by 1 Myr alternating colour bands. Black lines represent the extensive shear zones, red lines represent the compressive shear zones and dashed black and red lines represent the reactivated shear zones. The frictional shear zones are drawn for a corresponding plastic strain superior or equal to 1. The viscous shear zones are drawn for a corresponding viscous strain superior or equal to ~1.8-2. Abbreviations represent the passive margin domains, N.D.: Necking domain, H.E.: Hyper-Extended domain. Colours are the same than in the horizontal shortening legend.

Figure 6: Interpretative sketches based on models results. Narrow mantle exhumed domain rifts result in continental collision when inverted during hot geotherm. Wide mantle exhumed domain rifts result in obduction during inversion process with hot geotherms.

Table 1: Parameters used for Arrhenius flow laws.

## References


Albarède, F., Michard-Vitrac, A., 1978. Age and significance of the North Pyrenean metamorphism. Earth Planet. Sci. Lett. 40, 327–332. https://doi.org/10.1016/0012-821X(78)90157-7

Audet, P., Bürgmann, R., 2011. Dominant role of tectonic inheritance in supercontinent cycles. Nat. Geosci. 4, 184–187. https://doi.org/10.1038/ngeo1080

Ballato, P., Mulch, A., Landgraf, A., Strecker, M.R., Dalconi, M.C., Friedrich, A., Tabatabaei, S.H., 2010. Middle to late Miocene Middle Eastern climate from stable oxygen and carbon isotope data , southern Alborz mountains , N Iran. Earth Planet. Sci. Lett. 300, 125–138. https://doi.org/10.1016/j.epsl.2010.09.043

438 Beaumont, C., Jamieson, R.A., Butler, J.P., Warren, C.J., 2009. Crustal structure : A key
439 constraint on the mechanism of ultra-high-pressure rock exhumation. Earth Planet. Sci.
440 Lett. 287, 116–129. https://doi.org/10.1016/j.epsl.2009.08.001

441 Beaumont, C., Jamieson, R.A., Nguyen, M.H., Lee, B., 2001. Himalayan tectonics explained
442 by extrusion of a low-viscosity crustal channel coupled to focused surface denudation.
443 Nature 414, 738–742. https://doi.org/10.1038/414738a

444 Beltrando, M., Manatschal, G., Mohn, G., Dal Piaz, G.V., Vitale Brovarone, A., Masini, E.,
445 2014. Recognizing remnants of magma-poor rifted margins in high-pressure orogenic
446 belts: The Alpine case study. Earth-Science Rev. 131, 88–115.
447 https://doi.org/10.1016/j.earscirev.2014.01.001

448 Brune, S., Heine, C., Clift, P.D., Pérez-Gussinyé, M., 2017. Rifted margin architecture and
449 crustal rheology: Reviewing Iberia-Newfoundland, Central South Atlantic, and South
450 China Sea. Mar. Pet. Geol. 79, 257–281.
451 https://doi.org/10.1016/j.marpetgeo.2016.10.018

452 Brune, S., Heine, C., Pérez-Gussinyé, M., Sobolev, S. V., 2014. Rift migration explains
453 continental margin asymmetry and crustal hyper-extension. Nat. Commun. 5, 1–9.
454 https://doi.org/10.1038/ncomms5014

455 Burg, J., Gerya, T., 2005. The role of viscous heating in Barrovian metamorphism of
456 collisional orogens : thermomechanical models and application to the Lepontine Dome in
457 the Central Alps. J. Metamorph. Geol. 23, 75–95. https://doi.org/10.1111/j.1525-
458 1314.2005.00563.x

459 Burov, E., 2011. Rheology and strength of the lithosphere. Mar. Pet. Geol. 28, 1402–1443.
460 https://doi.org/10.1016/j.marpetgeo.2011.05.008

461 Burov, E., Diament, M., 1995. The effective elastic thickness (Te) of continental lithosphere:
462 What does it really mean? J. Geophys. Res. 100, 3905–3927.

463 Burov, E., Francois, T., Agard, P., Le, L., Meyer, B., Tirel, C., Lebedev, S., Yamato, P., Brun,
464 J., 2014. Rheological and geodynamic controls on the mechanisms of subduction and HP
465 / UHP exhumation of crustal rocks during continental collision : Insights from numerical
466 models. Tectonophysics 631, 212–250. https://doi.org/10.1016/j.tecto.2014.04.033

467 Burov, E., Jolivet, L., Le Pourhiet, L., Poliakov, A., 2001. A thermomechanical model of
468 exhumation of high pressure (HP) and ultra-high pressure (UHP) metamorphic rocks in
469 Alpine-type collision belts. Tectonophysics 342, 113–136.
470 https://doi.org/10.1016/S0040-1951(01)00158-5

471 Calignano, E., Sokoutis, D., Willingshofer, E., Gueydan, F., 2015a. Asymmetric vs .
472 symmetric deep lithospheric architecture of intra-plate continental orogens. Earth Planet.
473 Sci. Lett. 424, 38–50. https://doi.org/10.1016/j.epsl.2015.05.022

474 Calignano, E., Sokoutis, D., Willingshofer, E., Gueydan, F., Cloetingh, S., 2015b. Strain
475 localization at the margins of strong lithospheric domains: Insights from analog models.
476 Tectonics 1–17. https://doi.org/10.1002/2014TC003756.Received

477 Chenin, P., Manatschal, G., Picazo, S., Müntener, O., Karner, G., Johnson, C., Ulrich, M.,
478 2017. Influence of the architecture of magma-poor hyperextended rifted margins on
479 orogens produced by the closure of narrow versus wide oceans. Geosphere 13, 559–576.
480 https://doi.org/10.1130/GES01363.1

481 Clerc, C., Lagabrielle, Y., Neumaier, M., Reynaud, J.Y., De Saint Blanquat, M., 2012.
482 Exhumation of subcontinental mantle rocks: Evidence from ultramafic-bearing clastic
483 deposits nearby the Lherz peridotite body, French Pyrenees. Bull. la Soc. Geol. Fr. 183,

443–459. https://doi.org/10.2113/gssgfbull.183.5.443

Denèle, Y., Paquette, J.L., Olivier, P., Barbey, P., 2012. Permian granites in the Pyrenees: The Aya pluton (Basque Country). Terra Nov. 24, 105–113. https://doi.org/10.1111/j.1365-3121.2011.01043.x

Dick, H.J.B., 1989. Abyssal peridotites , very slow spreading ridges and ocean ridge magmatism Abyssal peridotites. Geol. Soc. London, Spec. Publ. 42, 71–105.

Ducoux, M., 2017. Structure, thermicité et évolution géodynamique de la Zone Interne Métamorphique des Pyrénées. University of Orléans.

Dumont, T., Replumaz, A., Rouméjon, S., Briais, A., Rigo, A., Bouillin, J.P., 2015. Microseismicity of the Béarn range: Reactivation of inversion and collision structures at the northern edge of the Iberian plate. Tectonics 34, 934–950. https://doi.org/10.1002/2014TC003816

Duretz, T., Gerya, T. V, 2013. Tectonophysics Slab detachment during continental collision : In fl uence of crustal rheology and interaction with lithospheric delamination. Tectonophysics 602, 124–140. https://doi.org/10.1016/j.tecto.2012.12.024

Duretz, T., Gerya, T. V, Kaus, B.J.P., Andersen, T.B., 2012. Thermomechanical modeling of slab eduction 117, 1–17. https://doi.org/10.1029/2012JB009137

Duretz, T., Petri, B., Mohn, G., Schmalholz, S.M., Schenker, F.L., Müntener, O., 2016. The importance of structural softening for the evolution and architecture of passive margins. Nat. Publ. Gr. 1–7. https://doi.org/10.1038/srep38704

Dymkova, D., Gerya, T., Burg, J., 2015. 2D thermomechanical modelling of continent – arc – continent collision. Gondwana Res. https://doi.org/10.1016/j.gr.2015.02.012

506 Erdös, Z., Huismans, R.S., Van Der Beek, P., Thieulot, C., 2014. Extensional inheritance and
507 surface processes as controlling factors of mountain belt structure. J. Geophys. Res.
508 Solid Earth 9042–9061. https://doi.org/10.1002/2014JB011408

509 Frets, E.C., Tommasi, A., Garrido, C., Vauchez, A., Mainprice, D., Kamaltarguisti, Amri, I.,
510 2014. The beni bousera peridotite (rif belt, morocco): An oblique-slip low-angle shear
511 zonethinning the subcontinental mantle lithosphere. J. Petrol. 55, 283–313.
512 https://doi.org/10.1093/petrology/egt067

513 Froitzheim, N., Rubatto, D., 1994. Continental breakup by detachment faulting : field
514 evidence and geochronological constraints (Tasna nappe, Switzerland). Terra Nov. 10,
515 171–176.

516 Grool, A.R., Ford, M., Vergés, J., Huismans, R.S., Christophoul, F., Dielforder, A., 2018.
517 Insights Into the Crustal-Scale Dynamics of a Doubly Vergent Orogen From a
518 Quantitative Analysis of Its Forelands: A Case Study of the Eastern Pyrenees. Tectonics
519 450–476. https://doi.org/10.1002/2017TC004731

520 Heron, P., Stephenson, R., Heron, P.J., Pysklywec, R.N., Stephenson, R., 2016. Identifying
521 mantle lithosphere inheritance in controlling intraplate orogenesis. J. Geophys. Res.
522 Solid Earth 121, 6966–6987. https://doi.org/10.1002/2016JB013460

523 Heron, P.J., Pysklywec, R.N., Stephenson, R., 2016. Lasting mantle scars lead to perennial
524 plate tectonics. Nat. Commun. 7, 1–7. https://doi.org/10.1038/ncomms11834

525 Hirth, G., Kohlstedt, D.L., 2003. Rheology of the Upper Mantle and the Mantle Wedge: A
526 View from the Experimentalists. Geophys. Monogr. 138, 83–105.

527 Hopper, J.R., Funck, T., 2004. Continental breakup and the onset of ultraslow seafloor
528 spreading off Flemish Cap on the Newfoundland rifted margin. Geology 32, 93–96.

https://doi.org/10.1130/G19694.1

Huismans, R.S., Buiter, S.J.H., Beaumont, C., 2005. Effect of plastic-viscous layering and strain softening on mode selection during lithospheric extension. J. Geophys. Res. B Solid Earth 110, 1–17. https://doi.org/10.1029/2004JB003114

Jamieson, R.A., Beaumont, C., 2013. On the origin of orogens. Bull. Geol. Soc. Am. 125, 1671–1702. https://doi.org/10.1130/B30855.1

Jammes, S., Huismans, R.S., 2012. Structural styles of mountain building: Controls of lithospheric rheologic stratification and extensional inheritance. J. Geophys. Res. B Solid Earth 117, 1–22. https://doi.org/10.1029/2012JB009376

Jammes, S., Huismans, R.S., Muñoz, J.A., 2014. Lateral variation in structural style of mountain building: Controls of rheological and rift inheritance. Terra Nov. 26, 201–207. https://doi.org/10.1111/ter.12087

Jammes, S., Manatschal, G., Lavier, L., Masini, E., 2009. Tectonosedimentary evolution related to extreme crustal thinning ahead of a propagating ocean: Example of the western Pyrenees. Tectonics 28, 1–24. https://doi.org/10.1029/2008TC002406

Jaquet, Y., Duretz, T., Grujic, D., Masson, H., Schmalholz, S.M., 2018. Formation of orogenic wedges and crustal shear zones by thermal softening , associated topographic evolution and application to natural orogens. Tectonophysics 746, 512–529. https://doi.org/10.1016/j.tecto.2017.07.021

Jourdon, A., Le Pourhiet, L., Petit, C., Rolland, Y., 2017. The deep structure and reactivation of the Kyrgyz Tien Shan: Modelling the past to better constrain the present. Tectonophysics. https://doi.org/10.1016/j.tecto.2017.07.019

551 Krawczyk, C.M., Reston, T.J., Beslier, M., Boillot, G., 1996. Evidence for detachment
552 tectonics on the Iberia Abyssal Plain rifted margin, in: Whitmarsh, R. et al. (Ed.),
553 Proceedings of the Ocean Drilling Program, Scientific Results. Texas, pp. 603–615.

554 Lafosse, M., Boutoux, A., Bellahsen, N., Le Pourhiet, L., 2018. Role of tectonic burial and
555 temperature on the inversion of inherited extensional basins during collision. Geol. Mag.
556 153, 811–826. https://doi.org/10.1017/S0016756816000510

557 Lagabrielle, Y., Bodinier, J.L., 2008. Submarine reworking of exhumed subcontinental mantle
558 rocks: Field evidence from the Lherz peridotites, French Pyrenees. Terra Nov. 20, 11–21.
559 https://doi.org/10.1111/j.1365-3121.2007.00781.x

560 Lagabrielle, Y., Labaume, P., De Saint Blanquat, M., 2010. Mantle exhumation, crustal
561 denudation, and gravity tectonics during Cretaceous rifting in the Pyrenean realm (SW
562 Europe): Insights from the geological setting of the lherzolite bodies. Tectonics 29, 1–26.
563 https://doi.org/10.1029/2009TC002588

564 Lagabrielle, Y., Lemoine, M., 1997. Alpine, Corsican and Apennine ophiolites: the slow-
565 spreading ridge model. Comptes Rendus l'Academie Sci. - Sci. la Terre des Planetes
566 325, 909–920.

567 Lavier, L.L., Manatschal, G., 2006. A mechanism to thin the continental lithosphere at
568 magma-poor margins. Nature 440, 324–328. https://doi.org/10.1038/nature04608

569 Le Pourhiet, L., Chamot-Rooke, N., Delescluse, M., May, D.A., Watremez, L., Pubellier, M.,
570 2018. Continental break-up of the South China Sea stalled by far-field compression. Nat.
571 Geosci. https://doi.org/10.1038/s41561-018-0178-5

572 Manatschal, G., 2014. New models for evolution of magma-poor rifted margins based on a
573 review of data and concepts from West Iberia and the Alps. Int. J. Earth Sci. 93, 432–

466. https://doi.org/10.1007/s00531-004-0394-7

Manatschal, G., Lavier, L., Chenin, P., 2015. The role of inheritance in forming and deforming hyper-extended rift systems and creating collisional orogens. Gondwana Res. 27, 140–164. https://doi.org/10.1127/1864-5658/2015-69

Masini, E., Manatschal, G., Tugend, J., Mohn, G., Flament, J.M., 2014. The tectono-sedimentary evolution of a hyper-extended rift basin: The example of the Arzacq-Mauléon rift system (Western Pyrenees, SW France). Int. J. Earth Sci. 103, 1569–1596. https://doi.org/10.1007/s00531-014-1023-8

May, D.A., Brown, J., Le Pourhiet, L., 2015. A scalable , matrix-free multigrid preconditioner for finite element discretizations of heterogeneous Stokes flow. Comput. Methods Appl. Mech. Eng. 290, 496–523. https://doi.org/10.1016/j.cma.2015.03.014

May, D.A., Brown, J., Le Pourhiet, L., 2014. pTatin3D : High-Performance Methods for Long-Term Lithospheric Dynamics. Proceeding SC′14 Proc. Int. Conf. High Perform. Comput. Networking, Storage Anal. 274–284.

Mesalles, L., Mouthereau, F., Bernet, M., Chang, C., Lin, A.T., Fillon, C., Sengelen, X., 2014. From submarine continental accretion to arc-continent orogenic evolution : The thermal record in southern Taiwan. Geology 42, 907–910. https://doi.org/10.1130/G35854.1

Molnar, P., Tapponnier, P., 1981. A possible dependence of tectonic strength on the age of the crust in Asia. Earth Planet. Sci. Lett. 52, 107–114. https://doi.org/10.1016/0012-821X(81)90213-2

Molnar, P., Tapponnier, P., 1975. Cenozoic Tectonics of Asia : Effects of a continental collision. Science (80-. ). 189, 419–426. https://doi.org/10.1126/science.189.4201.419

Montigny, R., Azambre, B., Rossy, M., Thuizat, R., 1986. K-Ar Study of cretaceous magmatism and metamorphism in the pyrenees: Age and length of rotation of the Iiberian Peninsula. Tectonophysics 129, 257–273. https://doi.org/10.1016/0040-1951(86)90255-6

Mouthereau, F., Filleaudeau, P.Y., Vacherat, A., Pik, R., Lacombe, O., Fellin, M.G., Castelltort, S., Christophoul, F., Masini, E., 2014. Placing limits to shortening evolution in the Pyrenees: Role of margin architecture and implications for the Iberia/Europe convergence. Tectonics 33, 2283–2314. https://doi.org/10.1002/2014TC003663

Mouthereau, F., Lacombe, O., Vergés, J., 2012. Building the Zagros collisional orogen : Timing , strain distribution and the dynamics of Arabia / Eurasia plate convergence. Tectonophysics 532–535, 27–60. https://doi.org/10.1016/j.tecto.2012.01.022

Mouthereau, F., Watts, A.B., Burov, E., 2013. Structure of orogenic belts controlled by lithosphere age. Nat. Geosci. 6, 1–5. https://doi.org/10.1038/ngeo1902

Müntener, O., Hermann, J., Trommsdorff, V., 2000. Cooling History and Exhumation of Lower- Crustal Granulite and Upper Mantle ( Malenco , Eastern Central Alps ). J. Petrol. 41, 175–200.

Müntener, O., Manatschal, G., Desmurs, L., Pettke, T., 2009. Plagioclase peridotites in ocean-continent transitions: Refertilized mantle domains generated by melt stagnation in the shallow mantle lithosphere. J. Petrol. 51, 255–294. https://doi.org/10.1093/petrology/egp087

Naliboff, J.B., Buiter, S.J.H., Péron-Pinvidic, G., Osmundsen, P.T., Tetreault, J., 2017. Complex fault interaction controls continental rifting. Nat. Commun. 1–9. https://doi.org/10.1038/s41467-017-00904-x

620 Précigout, J., Gueydan, F., Garrido, C.J., Cogné, N., Booth-Rea, G., 2013. Deformation and
621 exhumation of the Ronda peridotite (Spain). Tectonics 32, 1011–1025.
622 https://doi.org/10.1002/tect.20062

623 Ranalli, G., Murphy, D.C., 1987. Rheological stratification of the lithosphere. Tectonophysics
624 132, 281–295.

625 Reston, T.J., Leythaeuser, T., Booth-Rea, G., Sawyer, D., Klaeschen, D., Long, C., 2007.
626 Movement along a low-angle normal fault: The S reflector west of Spain. Geochemistry,
627 Geophys. Geosystems 8, 1–14. https://doi.org/10.1029/2006GC001437

628 Reston, T.J., Mcdermott, K.G., 2011. Successive detachment faults and mantle unroofi ng at
629 magma-poor rifted margins. Geology 39, 1071–1074. https://doi.org/10.1130/G32428.1

630 Rybacki, E., Dresen, G., 2000. Dislocation and diffusion creep of synthetic anorthite
631 aggregates. J. Geophys. Res. Solid Earth 105, 26017–26036.
632 https://doi.org/10.1029/2000JB900223

633 Sauter, D., Cannat, M., Rouméjon, S., Andreani, M., Birot, D., Bronner, A., Brunelli, D.,
634 Carlut, J., Delacour, A., Guyader, V., Macleod, C.J., Manatschal, G., Mendel, V.,
635 Ménez, B., Pasini, V., Ruellan, E., Searle, R., 2013. Continuous exhumation of mantle-
636 derived rocks at the Southwest Indian Ridge for 11 million years. Nat. Geosci. 6, 314–
637 320. https://doi.org/10.1038/ngeo1771

638 Sauter, D., Rommevaux-Jestin, C., Parson, L.M., Fujimoto, H., Mével, C., Cannat, M.,
639 Tamaki, K., 2004. Focused magmatism versus amagmatic spreading along the ultra-slow
640 spreading Southwest Indian Ridge: Evidence from TOBI side scan sonar imagery.
641 Geochemistry, Geophys. Geosystems 5, 1–20. https://doi.org/10.1029/2004GC000738

642 Teixell, A., Labaume, P., Lagabrielle, Y., 2016. The crustal evolution of the west-central

643 Pyrenees revisited: Inferences from a new kinematic scenario. Comptes Rendus - Geosci.
644 348, 257–267. https://doi.org/10.1016/j.crte.2015.10.010

645 Tetreault, J.L., Buiter, S.J.H., 2017. The influence of extension rate and crustal rheology on
646 the evolution of passive margins from rifting to break-up. Tectonophysics 0–1.
647 https://doi.org/10.1016/j.tecto.2017.08.029

648 Tugend, J., Manatschal, G., Kusznir, N.J., Masini, E., Mohn, G., Thinon, I., 2014. Formation
649 and deformation of hyperextended rift systems: Insights from rift domain mapping in the
650 Bay of Biscay-Pyrenees. Tectonics 1239–1276.
651 https://doi.org/10.1002/2014TC003529.Received

652 Vacherat, A., Mouthereau, F., Pik, R., Bellahsen, N., Gautheron, C., Bernet, M., Daudet, M.,
653 Balansa, J., Tibari, B., Jamme, R.P., Radal, J., 2016. Rift-to-collision transition recorded
654 by tectonothermal evolution of the northern Pyrenees. Tectonics 35, 907–933.
655 https://doi.org/10.1002/2015TC004016

656 Vacherat, A., Mouthereau, F., Pik, R., Bernet, M., Gautheron, C., Masini, E., Pourhiet, L. Le,
657 Tibari, B., Lahfid, A., 2014. Thermal imprint of rift-related processes in orogens as
658 recorded in the Pyrenees. Earth Planet. Sci. Lett. 408, 296–306.
659 https://doi.org/10.1016/j.epsl.2014.10.014

660 Velasque, P.C., Ducasse, L., Muller, J., Scholten, R., 1989. The influence of inherited
661 extensional structures on the tectonic evolution of an intracratonic chain : the example of
662 the Western Pyrenees. Tectonophysics 162, 243–264.

663 Wang, Y., Chevrot, S., Monteiller, V., Komatitsch, D., Mouthereau, F., Manatschal, G., 2016.
664 The deep roots of the western Pyrenees revealed by full waveform inversion of
665 teleseismic P waves. Geology 44, 475–478. https://doi.org/10.1130/G37812.1

Warren, C.J., Beaumont, C., Jamieson, R.A., 2008. Modelling tectonic styles and ultra-high pressure ( UHP ) rock exhumation during the transition from oceanic subduction to continental collision. Earth Planet. Sci. Lett. 267, 129–145. https://doi.org/10.1016/j.epsl.2007.11.025

Watremez, L., Burov, E., D'Acremont, E., Leroy, S., Huet, B., Le Pourhiet, L., Bellahsen, N., 2013. Buoyancy and localizing properties of continental mantle lithosphere: Insights from thermomechanical models of the eastern Gulf of Aden. Geochemistry, Geophys. Geosystems 14, 2800–2817. https://doi.org/10.1002/ggge.20179

Wickham, S.M., 1987. Crustal anatexis and granite petrogenesis during low-pressure regional metamorphism: The trois seigneurs massif, pyrenees, France. J. Petrol. 28, 127–169. https://doi.org/10.1093/petrology/28.1.127

Yamato, P., Burov, E., Agard, P., Le Pourhiet, L., Jolivet, L., 2008. HP-UHP exhumation during slow continental subduction: Self-consistent thermodynamically and thermomechanically coupled model with application to the Western Alps. Earth Planet. Sci. Lett. 271, 63–74. https://doi.org/10.1016/j.epsl.2008.03.049

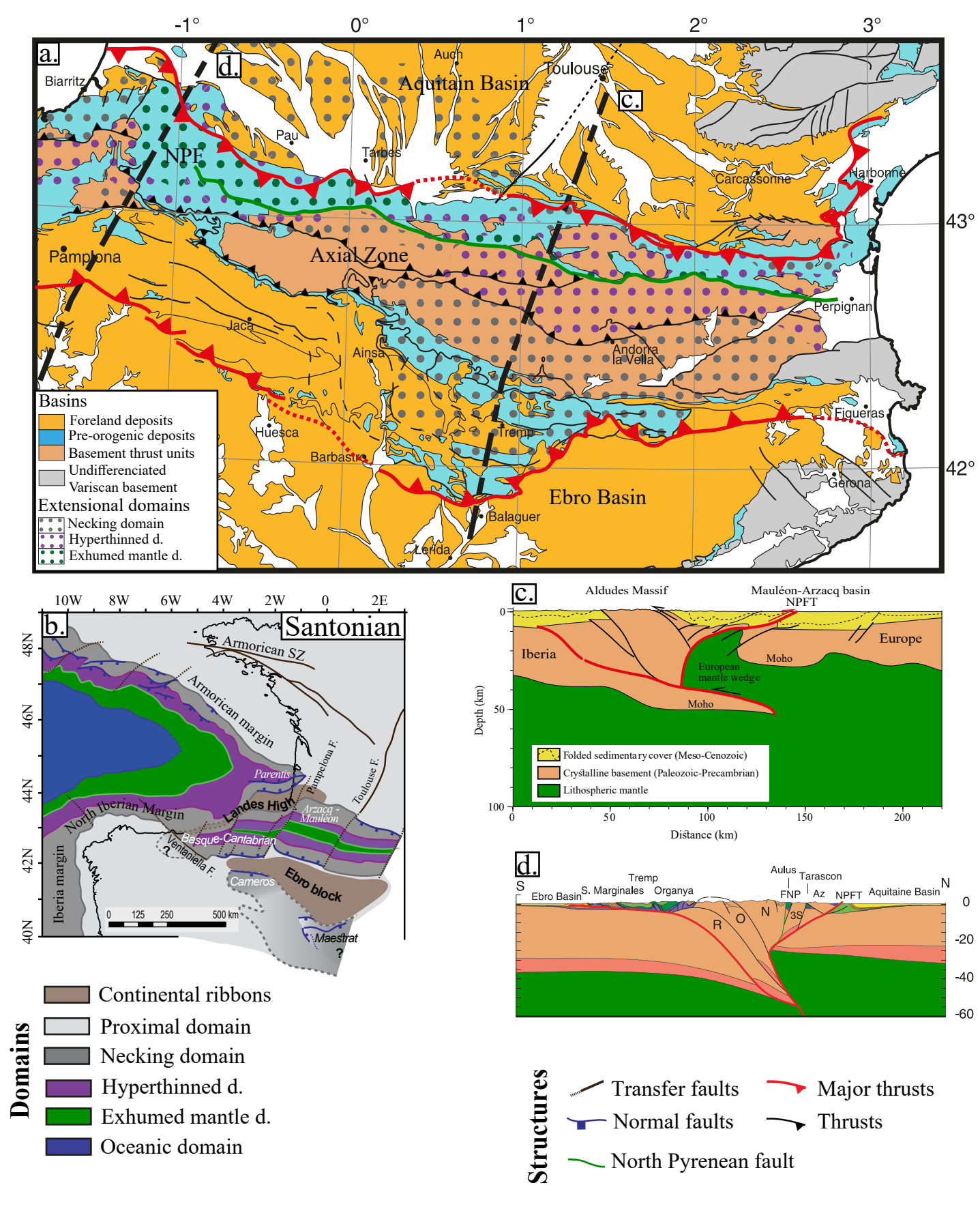
a.
-1°
0°
1°
2°
3°
43°
42°
Biarritz
Auch
Toulouse
Aquitain Basin
d.
c.
Pau
Tarbes
NPF
Carcassonne
Narbonne
Pamplona
Axial Zone
Perpignan
Jaca
Ainsa
Andorra la Vella
Figueras
Huesca
Tremp
Barbastro
Gerona
Ebro Basin
Balaguer
Lerida
Basins
Foreland deposits
Pre-orogenic deposits
Basement thrust units
Undifferenciated Variscan basement
Extensional domains
Necking domain
Hyperthinned d.
Exhumed mantle d.
b.
Santonian
10W
8W
6W
4W
2W
0
2E
48N
46N
44N
42N
40N
Armorican SZ
Armorican margin
Parentis
Pampelona F.
Toulouse F.
Landes High
Arzacq - Mauléon
North Iberian Margin
Basque-Cantabrian
Ventaniella F.
Cameros
Ebro block
Iberia margin
Maestrat
0 125 250 500 km
c.
Aldudes Massif
Mauléon-Arzacq basin
NPFT
Europe
Iberia
Moho
European mantle wedge
Moho
Depth (km)
0
50
100
0
50
100
150
200
Distance (km)
Folded sedimentary cover (Meso-Cenozoic)
Crystalline basement (Paleozoic-Precambrian)
Lithospheric mantle
d.
S
N
Ebro Basin
Tremp
S. Marginales
Organya
Aulus
Tarascon
FNP
Az
NPFT
Aquitaine Basin
R
O
N
3S
0
-20
-40
-60
Domains
Continental ribbons
Proximal domain
Necking domain
Hyperthinned d.
Exhumed mantle d.
Oceanic domain
Structures
Transfer faults
Major thrusts
Normal faults
Thrusts
North Pyrenean fault

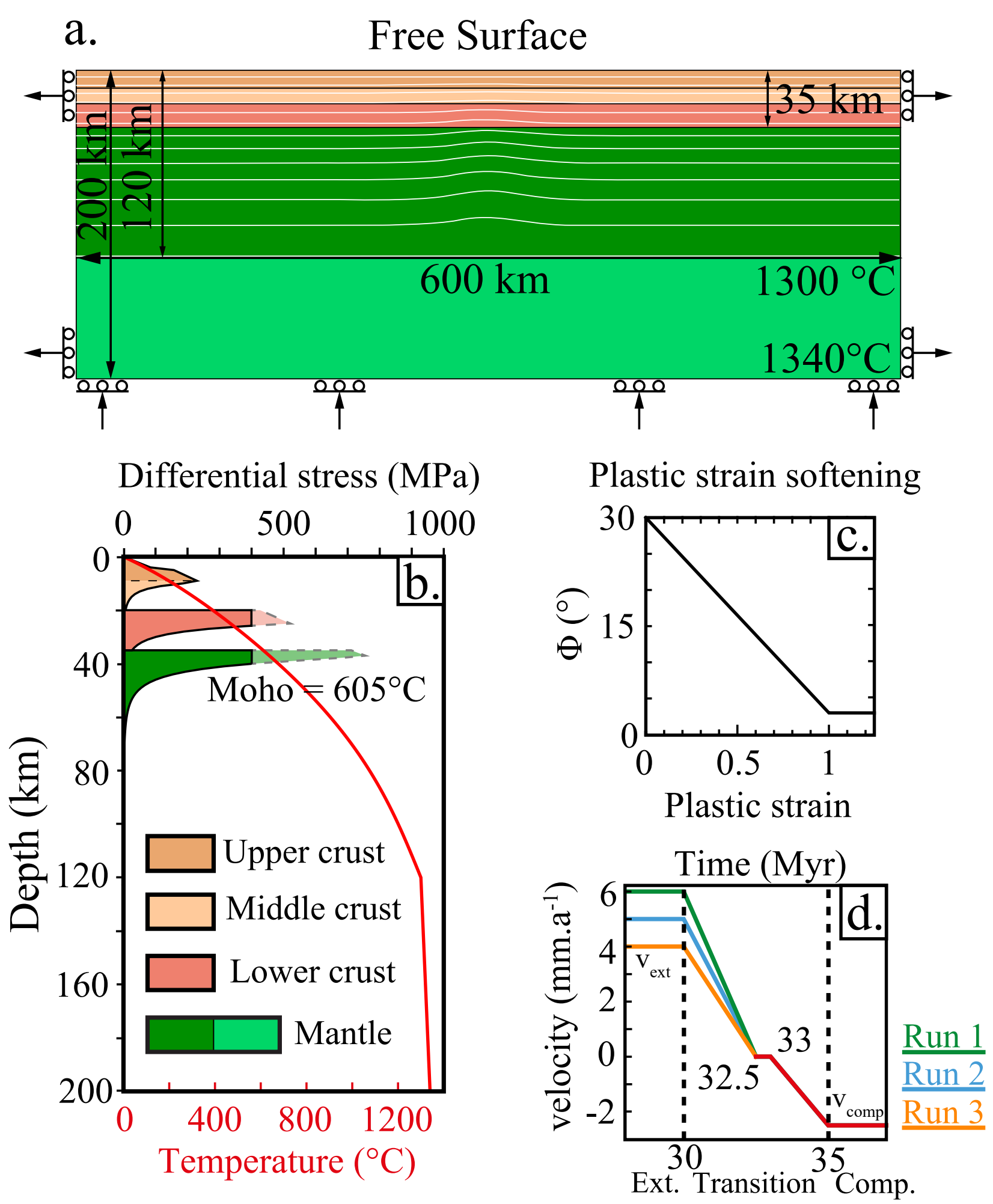
a.
Free Surface
35 km
200 km
120 km
600 km
1300 °C
1340°C
Differential stress (MPa)
0
500
1000
b.
Moho = 605°C
Depth (km)
0
40
80
120
160
200
Upper crust
Middle crust
Lower crust
Mantle
0
400
800
1200
Temperature (°C)
Plastic strain softening
c.
Φ (°)
30
15
0
0
0.5
1
Plastic strain
Time (Myr)
d.
velocity (mm.a-1)
6
4
2
0
-2
Vext
33
32.5
Vcomp
Run 1
Run 2
Run 3
30
35
Ext.
Transition
Comp.

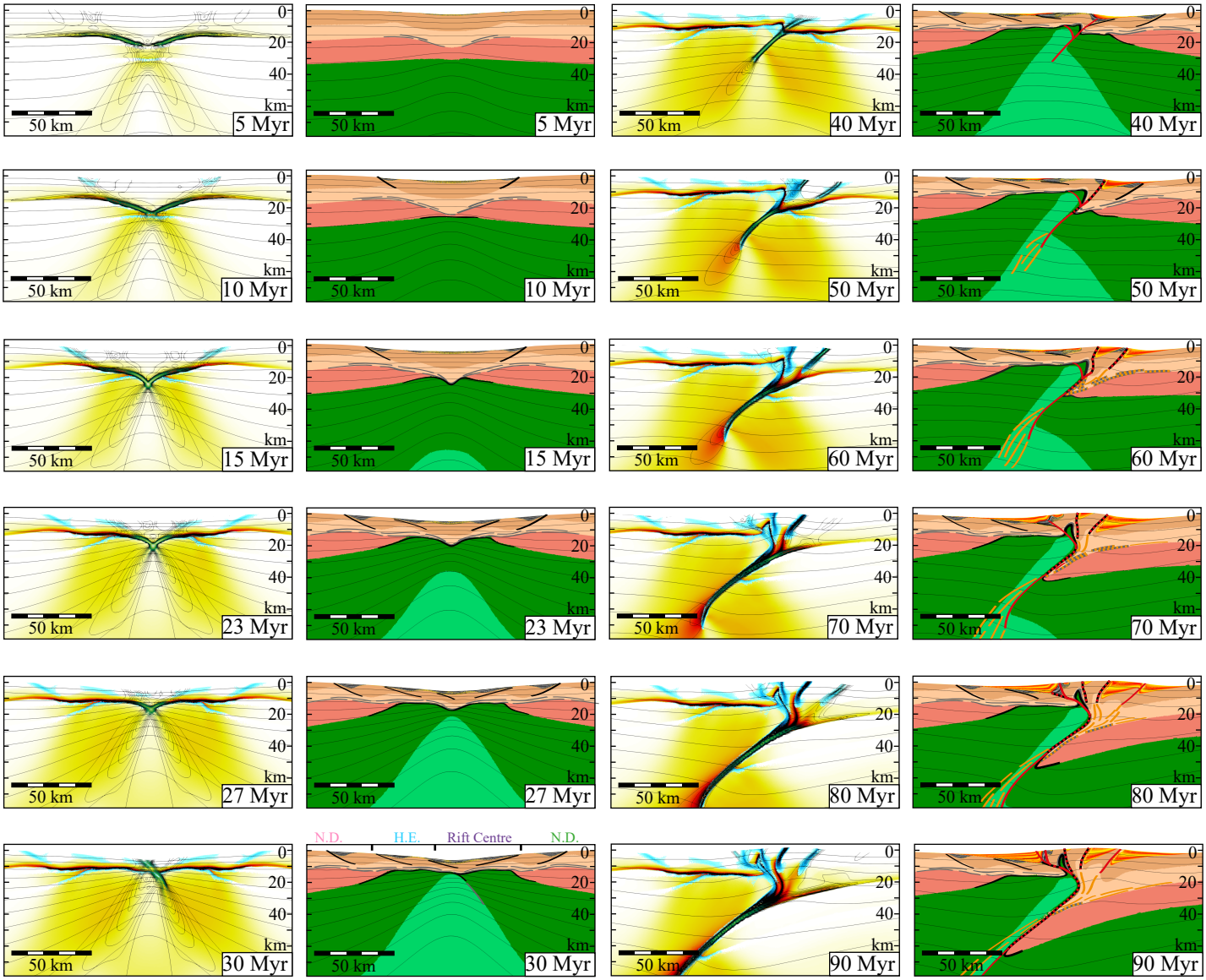


Numerical results:

Plastic Strain

0 1 2 3 4 5 6

Viscous Strain

0 1 2 3 4 5 6

Strain Rate Second Invariant ($s^{-1}$)

$5x10^{-15}$ $1x10^{-14}$ $2x10^{-14}$ $5x10^{-14}$

Age of sediments (Myr)

0 40 90

Syn-rift Syn-orogenic

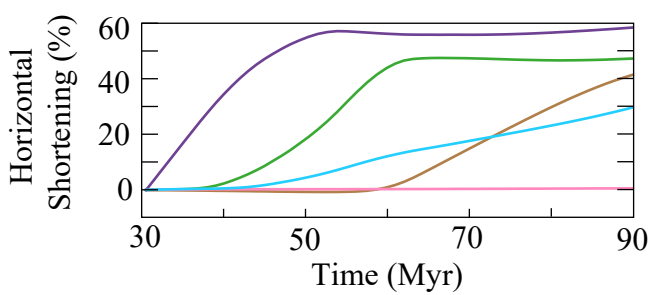


Deformation interpretation:

- Frictionnal extensive shear zone
- Frictionnal reactivated shear zone
- Frictionnal compressive shear zone
- Viscous extensive shear zone
- Viscous reactivated shear zone
- Viscous compressive shear zone

- Lower plate proximal domain
- Lower plate necking domain
- Rift centre
- Upper plate necking domain
- Upper plate Hyper extended domain

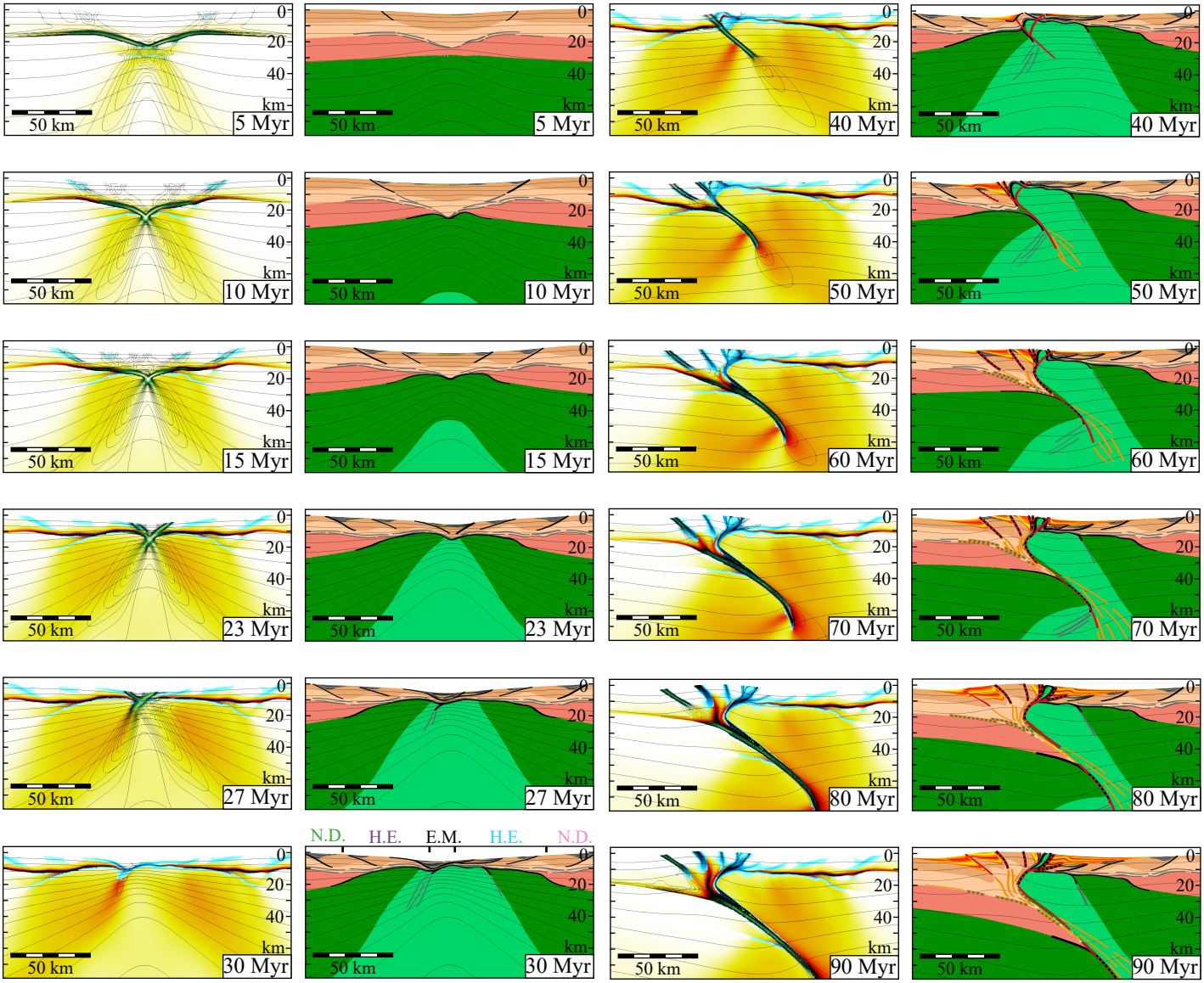


Numerical results:

Plastic Strain

0 1 2 3 4 5 6

Viscous Strain

0 1 2 3 4 5 6

Strain Rate Second Invariant ($s^{-1}$)

$5x10^{-15}$ $1x10^{-14}$ $2x10^{-14}$ $5x10^{-14}$

Age of sediments (Myr)

0 40 90

Syn-rift Syn-orogenic

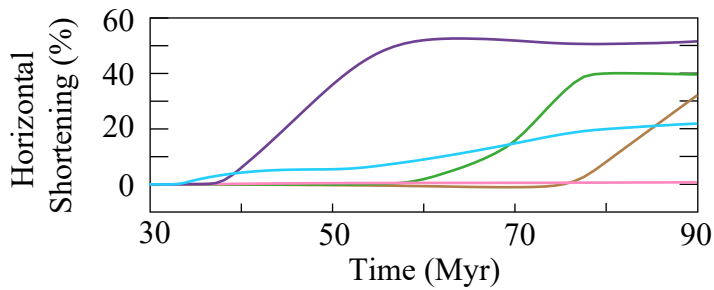


Deformation interpretation:

- Frictionnal extensive shear zone
- Frictionnal reactivated shear zone
- Frictionnal compressive shear zone
- Viscous extensive shear zone
- Viscous reactivated shear zone
- Viscous compressive shear zone

- Lower plate proximal domain
- Lower plate necking domain
- Lower plate Hyper extended domain
- Upper plate necking domain
- Upper plate Hyper extended domain

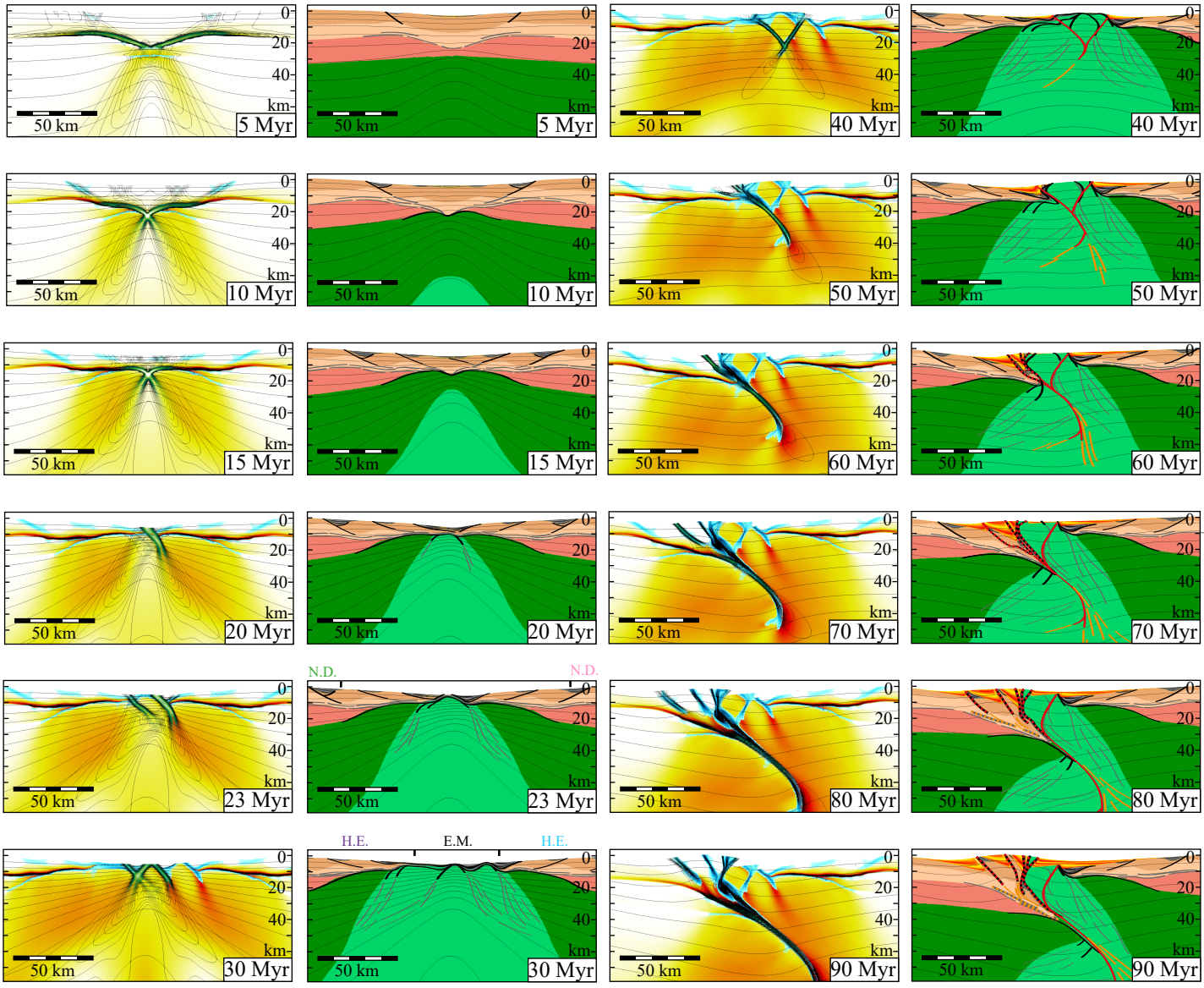


Numerical results:

Plastic Strain

0 1 2 3 4 5 6

Strain Rate Second Invariant ($s^{-1}$)

$5x10^{-15}$ $1x10^{-14}$ $2x10^{-14}$ $5x10^{-14}$

Viscous Strain

0 1 2 3 4 5 6

Age of sediments (Myr)

0 40 90

Syn-rift Syn-orogenic

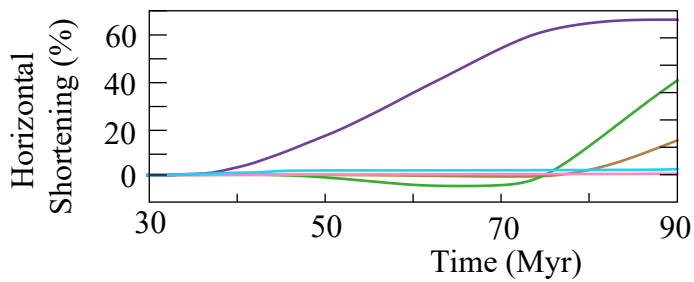


Deformation interpretation:

- Frictionnal extensive shear zone
- Frictionnal reactivated shear zone
- Frictionnal compressive shear zone
- Viscous extensive shear zone
- Viscous reactivated shear zone
- Viscous compressive shear zone

- Lower plate proximal domain
- Lower plate necking domain
- Lower plate Hyper extended domain
- Upper plate necking domain
- Upper plate Hyper extended domain

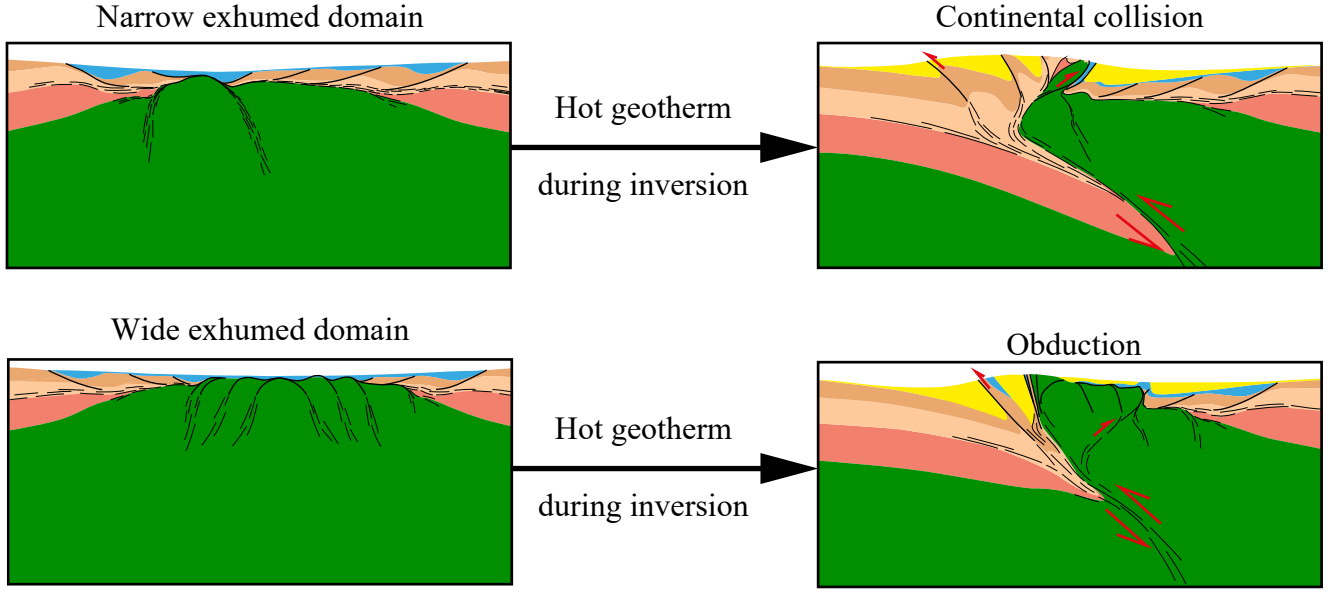
Narrow exhumed domain
Continental collision
Hot geotherm
during inversion
Wide exhumed domain
Obduction
Hot geotherm
during inversion